ACS APPLIED NANO MATERIALS
Cite This: ACS Appl. Nano Mater. 2019, 2, 6804−6808
Letter
www.acsanm.org

Pressure-Induced Transformations of Three-Component Heterostructural Nanocrystals with CdS−Au_2S Janus Nanoparticles as Hosts and Small Au Nanoparticles as Satellites

Hua Zhu,[†] Tong Cai,[†] Yucheng Yuan,[†] Xudong Wang,[‡] Yasutaka Nagaoka,[†] Jing Zhao,[‡] Zhenxian Liu,[⊥] Ruipeng Li,[§] and Ou Chen*[,†]

[†]Department of Chemistry, Brown University, Providence, Rhode Island 02912, United States
[‡]Department of Chemistry, University of Connecticut, Storrs, Connecticut 06269, United States
[⊥]Department of Physics, University of Illinois at Chicago, Illinois 60607-7059, United States
[§]National Synchrotron Light Source II, Brookhaven National Laboratory, Upton, New York 11973, United States

Supporting Information

ABSTRACT: Heterostructural nanocrystals (HNCs) have drawn enormous attention because of the combined and synergistic properties inherited from their individual components and interactions. Here we design a three-component CdS−Au_2S−Au Janus-satellite HNC to study the pressure process of HNC superlattices (HNC-SLs). In situ small/wide-angle X-ray scattering shows that the HNC-SLs can undergo structural transformations at both atomic and meso scales. At the same time, CdS−Au_2S−Au Janus-satellite HNCs can morphologically transform into CdS−Au_2S−Au heterotrimer HNCs through intraparticle migration and coalescence of Au satellites. Our results demonstrate that pressure can be employed as a clean and efficient way to fabricate complex heterostructural nanomaterials suitable for potential applications in photocatalysis and theranostics.

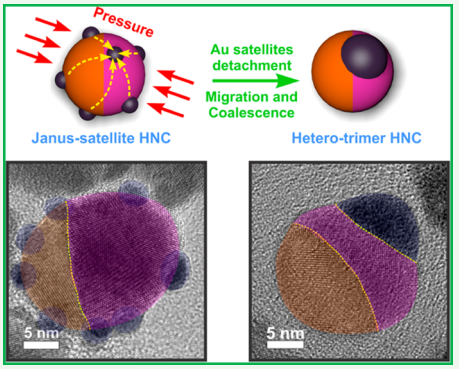

KEYWORDS: *high-pressure processing, heterostructural nanocrystal, heterotrimer, coalescence, nanocrystal superlattice*

Heterostructural nanocrystals (HNCs) with precisely defined sizes, shapes, and compositional boundaries are a subclass of colloidal nanocrystals (NCs) containing multiple chemically distinct components.[1−6] HNCs show a great potential to exhibit combined and synergistic properties inherited from their individual constituents, such as optical and electronic coupling and enhanced catalytic performance.[7−9] Moreover, chemically distinct domains of HNCs provide an opportunity to not only diversify their functionalities but also uniquely self-organize them into novel superstructures with an unprecedented level of structural and property control.[10−13]

Although single-component colloidal NCs can be readily synthesized with high uniformity, colloidal synthesis of HNCs with controlled geometries has always been challenging. Current synthetic strategies usually rely on a selective seeded growth method, which heavily involves chemical treatments and purifications, largely limited by material-specific preferences.[14] Recently, high pressure processing has proven to be a fast and chemical-orthogonal way to fabricate novel nanomaterials.[15−21] Besides phase transition at the atomic scale, previous studies have shown that high-pressure treatment can manipulate the electronic properties of semiconductor NCs and induce morphological transformation of NCs through a stress-driven "pressure-sintering" process.[5,22,23]

Here, we specially designed three-component CdS−Au_2S−Au Janus-satellite HNCs with CdS−Au_2S Janus particles as hosts and small Au particles as satellites (Scheme 1). We studied the high-pressure behavior of HNC superlattices (HNC-SLs) using a diamond anvil cell (DAC) technique.[16] During a full pressure cycle of 0−12.7 GPa, Au satellites detached, migrated, and coalesced on the surface of HNCs and finally transformed into CdS−Au_2S−Au heterotrimer NCs (Scheme 1). Our study demonstrated that the deviatoric stress enabled by external high pressure can serve as a clean and efficient way to fabricate highly complex heterostructural nanomaterials that cannot be easily achieved through conventional synthetic avenues. The as-synthesized three-component CdS−Au_2S−Au heterotrimer NCs provide a unique nanostructural platform suitable for a range of applications from heterogeneous photocatalysis to multifunctional theranostics.[24]

We employed a two-step method to syntheisze CdS−Au_2S−Au Janus-satellite HNCs. Briefly, CdS−$Cu_{1.8}S$ NCs were synthesized using a modified literature method, followed by a Cu^+-to-Au^+ cation-exchange process (Scheme 1).[25] Because the Cu^+ ion possesses much higher ion mobility than Cd^{2+},

Received: September 25, 2019
Accepted: October 25, 2019
Published: October 25, 2019

DOI: 10.1021/acsanm.9b01860
ACS Appl. Nano Mater. 2019, 2, 6804−6808

Scheme 1. Schematic Illustration of the Synthetic Strategy of Three-Component CdS−Au_2S−Au Janus-Satellite HNCs and the Pressure-Induced Transformation[a]

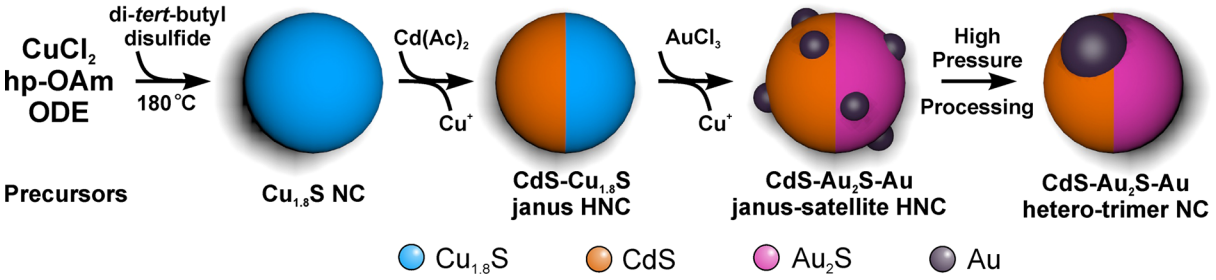

[a]hp-OAm represents high-purity oleylamine, and ODE represents 1-octadecene.

only the $Cu_{1.8}S$ side can be exchanged to form Au_2S.[26,27] Meanwhile, small Au satellites grew onto the HNC surface by the addition of an extra amount of Au precursor (Scheme 1 and see also details in the Supporting Information, SI). The UV−vis absorption spectrum of the obtained CdS−Au_2S−Au Janus-satellite HNCs showed an increased absorbance in the visible range of 400−700 nm, which can be attributed to the localized surface plasmon resonance from the Au satellites as well as the absorbance from the Au_2S domain of the HNCs (Figure 1a).[28] The successful cation exchange was further confirmed by decreased absorbance in the near-IR range (800−1500 nm), which arose solely from the $Cu_{1.8}S$ side of the HNCs before the occurrence of cation exhange (Figure 1a). Transmission electron microscopy (TEM) measurements showed the monodisperse CdS−Au_2S−Au HNCs with uniform sizes of both the CdS−Au_2S Janus hosts (19.8 ± 1.3 nm) and Au satellites (3.6 ± 0.8 nm) (Figures 1b and S1 and S2).

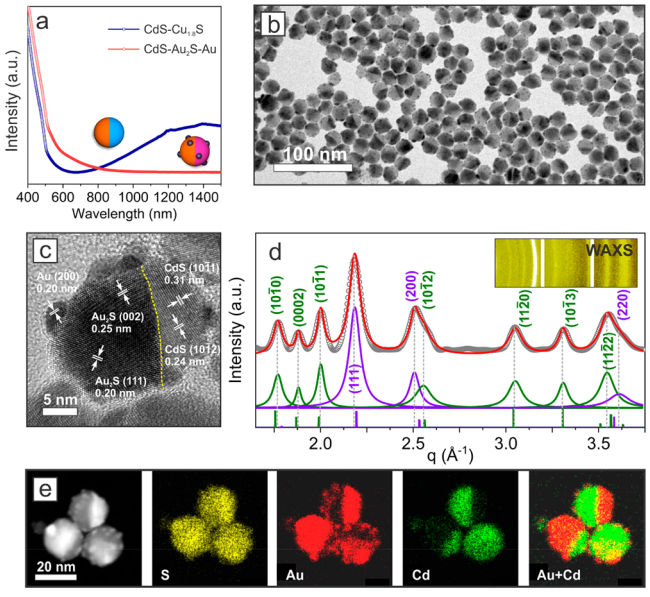

Figure 1. Characterization of CdS−Au_2S−Au Janus-satellite HNCs. (a) Absorption spectrum before and after Au cation exchange and growth. (b) Representative TEM image and (c) a HR-TEM image of as-synthesized CdS−Au_2S−Au Janus-satellite HNCs. (d) Integrated WAXS pattern of the HNCs. The original WAXS peaks and fitted peaks of WZ−CdS and Au_2S are labeled in green and purple, respectively. Inset: Corresponding 2D pattern. (e) HAADF-STEM image and elemental mapping (S, Au, and Cd) of as-synthesized HNCs.

High-resolution TEM (HR-TEM) images clearly displayed the single-crystalline nature of both the CdS and Au_2S domains (Figures 1c and S3 and S4). Moreover, the observations of atomic fringes crossing the interfaces between three chemical components (i.e., CdS, Au_2S, and Au) indicate their epitaxial growth nature of the HNCs (Figures 1c and S3 and S4). For example, the Au_2S $(200)_{Au_2S}$ planes showed a direct connection to the CdS $(10\bar{1}2)_{CdS}$ planes (Figure 1c). The wide-angle X-ray scattering (WAXS) pattern of the sample showed that the CdS domain preserved a wurtzite (WZ) crystal structure after Au^+ cation exchange and satellite growth (Figure 1d). Meanwhile, a set of additional peaks can be assigned to $(111)_{Au_2S}$, $(200)_{Au_2S}$, and $(220)_{Au_2S}$ Bragg diffraction features with a calculated lattice parameter of 4.98 Å, ∼1.0% smaller than the bulk value (Figure 1d and Table S1).[29] No clear peaks from Au satellites can be observed in the WAXS pattern, which is due to their small domain size compared to the CdS−Au_2S hosts (3.6 vs 19.8 nm). Finally, high-angle annular dark-field scanning TEM (HAADF-STEM) images and elemental mapping results (Figure 1e) showed the Janus-satellite type of heterostructure, further confirming the unique Janus-satellite architecture of the three-component CdS−Au_2S−Au HNCs.

HNC-SLs were fabricated through a controlled solvent evaporation process (see the SI). The resulting superstructure exhibits a face-centered-cubic (fcc) structure (Figure 2a). Interestingly, the wide-angle electron diffraction (WAED) pattern showed a localized signal, indicating the presence of atomic orientational alignments of the HNC-SL (Figure 2b). The integrated small-angle X-ray scattering (SAXS) plot confirmed the fcc structure with well-defined diffraction peaks (Figure 2c). The lattice parameter was calculated as 30.53 ± 0.50 nm with the nearest inter-NC distance of 21.59 ± 0.35 nm (Table S2). Given the size of CdS−Au_2S−Au HNCs, the surface-to-surface distance of the HNC hosts can be determined as 1.79 nm, in line with previous reports suggesting a ligand intercalation behavior in the HNC-SL studied here.[11,30]

In situ SAXS and WAXS of the HNC-SLs were simultaneously monitored while applying a high-pressure cycle inside a DAC. Upon compression, all of the SAXS peaks shifted to lower q values with an increase of the pressure from 0.0 to 12.7 GPa (Figure 3a). The entire process was accompanied by a gradual peak-broadening effect, and the fcc superlattice (SL) gradually transformed into a *lamellar* structure (Figures 3a and S6 and Table S3). The reversed peak shifts were observed during the pressure-release process, and the *lamellar* structure was largely retained after total

DOI: 10.1021/acsanm.9b01860
ACS Appl. Nano Mater. 2019, 2, 6804−6808

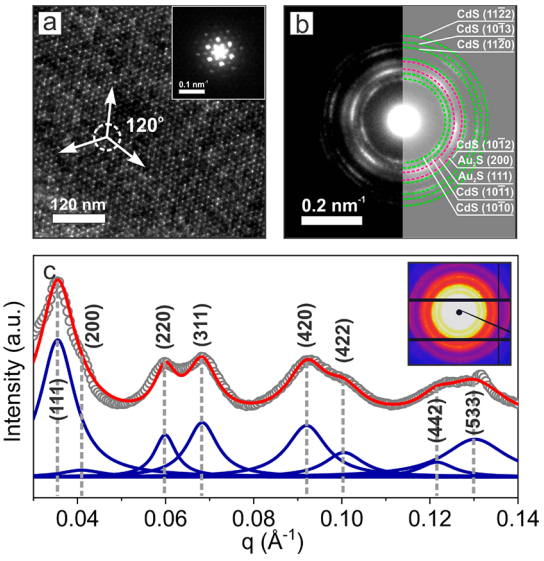

Figure 2. (a) Representative TEM image of self-assembled HNC-SLs. Inset: Corresponding selected-area electron diffraction pattern. (b) Corresponding WAED pattern showing a localized signal. (c) Integrated SAXS pattern of the HNC-SLs. The original spectrum, fitted SAXS pattern, and constituent peaks are shown in gray, red, and blue, respectively. Inset: Corresponding 2D SAXS image.

release of the pressure (Figure 3a). This irreversible superstructural evolution indicated migrations of the HNC surface ligands during the pressure cycle and morphological transformations of individual CdS−Au_2S−Au HNCs.[5,15,22] Meanwhile, atomic crystal phase transitions were also detected by in situ WAXS measurements (Figure 3b). Upon an increase of the pressure, all of the WAXS peaks shifted to higher q values, indicating lattice shrinkage under high pressure. The WZ structure of the CdS domain was maintained up to ∼5.2 GPa before it transformed to a rock-salt (RS) phase (Figure 3b).[31] The RS phase of CdS then remained while the pressure was increased to 12.7 GPa and then released to ambient conditions (Figure 3c,d). In contrast, the Au_2S domain continued to contract upon an increase of the pressure, with no obvious phase transition occurring. Upon total release of the pressure, the Au_2S lattice parameter largely bounced back to the value of 4.97 Å, but the CdS domain remained as the high-pressure RS phase (Figure 3c and Table S4). On the basis of in situ structural characterization, volumetric compression as a function of the pressure gave bulk moduli (B_0) of 40.4, 56.1, and 120.8 GPa for Au_2S, WZ−CdS, and RS−CdS, respectively, following the second-order Birch−Murnaghan equation of state (Figure 3e). All of the calculated B_0 values are generally larger than those reported for bulk materials, consistent with previous observations.[31,32]

Markedly, after the pressure cycle, a set of new scattering peaks located at d spacings of 2.34 and 2.02 Å emerged (Figure 3b,c), which matched well with those of the bulk Au $(111)_{Au}$ and $(200)_{Au}$ values (Figure 3b,c and Table S4). An average domain size of ∼9.5 nm was determined through the Scherrer equation calculation (Table S4). This observation indicated that Au domains with a larger size than the initial Au satellites (∼3.6 nm) were formed after pressurization, which was most likely due to an Au−S bond-breaking process, followed by an intraparticle Au atomic movement at the HNC surfaces under external high pressure.[5]

In order to confirm the morphological change of CdS−Au_2S−Au HNCs, TEM measurements were carried out for the pressurized sample collected from the DAC. TEM images showed that the HNCs indeed transformed from the initial Janus-satellite-type morphology to the final heterotrimer architecture (Figures 4a,b and S7). HR-TEM images showed clear domain boundaries between three distinct chemical components (i.e., CdS, Au_2S, and Au; Figure 4c,d). Mean-

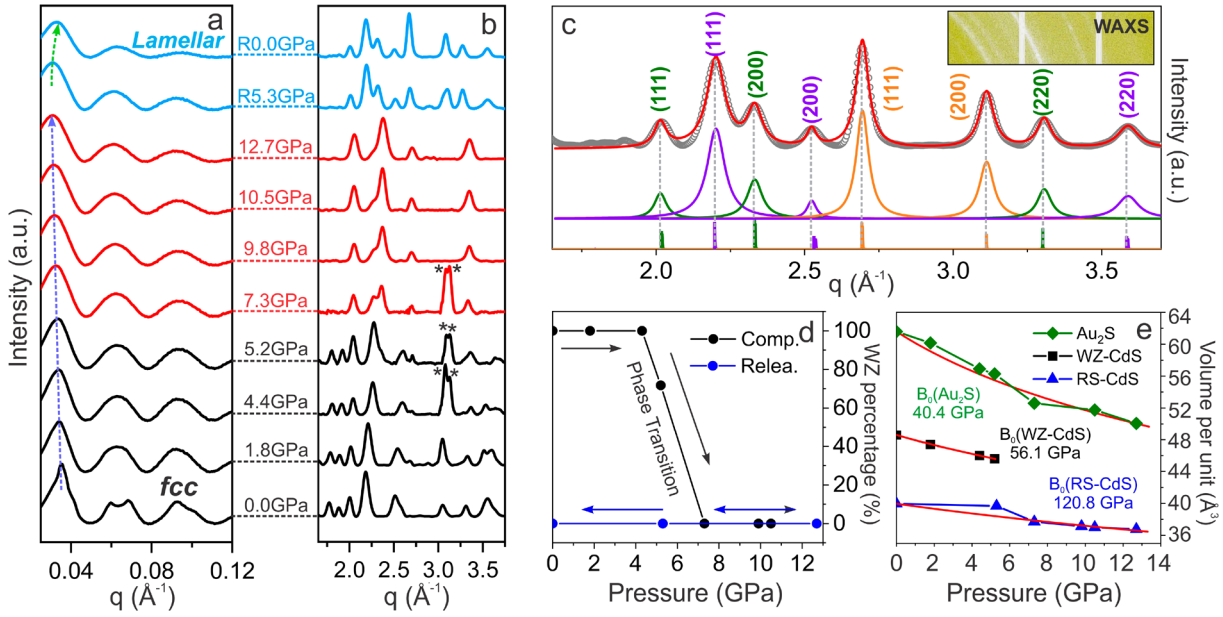

Figure 3. Structural evolution of the HNCs and HNC-SLs under high pressure. (a and b) In situ SAXS and WAXS patterns during the whole pressure cycle. The signals from the gasket are labeled by asterisks. (c) Integrated WAXS patterns of the pressurized CdS−Au_2S−Au HNCs. The WAXS peaks of RS−CdS, Au_2S, and Au are labeled in green, purple, and orange, respectively. Inset: Corresponding 2D WAXS pattern. (d) WZ phase percentage of CdS as a function of the pressure. (e) Bulk moduli calculated using the second-order Birch−Murnaghan equation of state based on the volumetric evolution of unit cells per chemical unit as a function of the pressure.

DOI: 10.1021/acsanm.9b01860
ACS Appl. Nano Mater. 2019, 2, 6804−6808

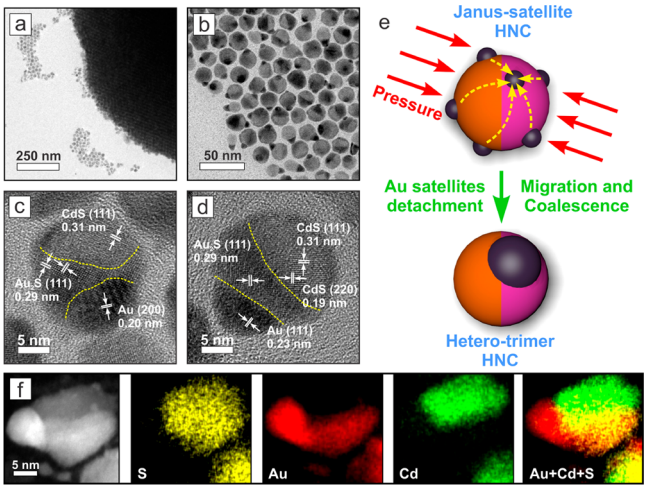

Figure 4. Characterization of the pressurized CdS−Au_2S−Au HNCs after pressure. (a and b) Representative TEM images of a pressurized sample before and after dispersion. (c and d) HR-TEM images of the heterotrimers. The CdS-preserved RS structure and Au showed a single-crystalline feature. (e) Schematic illustration of the pressure-sintering process. (f) HAADF-STEM image and elemental mapping (S, Au, and Cd) of the heterotrimers after pressure.

while, the measured *d* spacings of 3.1 and 1.9 Å for the CdS domain could be assigned to the RS $(111)_{CdS}$ and $(220)_{CdS}$, consistent with the WAXS data (Figures 4c,d and 3c). In addition, the measured *d* spacings of 2.9, 2.3, and 2.0 Å can be assigned to $(111)_{Au_2S}$, $(111)_{Au}$, and $(200)_{Au}$, respectively (Figure 4c,d). Interestingly, most of the newly formed Au islands (>95%) showed single-crystalline nature with an average diameter of ∼9.0 nm, in good agreement with the calculated value (∼9.5 nm) based on the WAXS data (Figure 3c and Table S4). HAADF-STEM and elemental mapping measurements further confirmed the heterotrimer morphology of the pressurized CdS−Au_2S−Au HNCs (Figures 4d and S8). The Au islands showed preferential locations either on the Au_2S side or at the Au_2S/CdS interface (Figures 4b and S7). We hypothesize that, while CdS and Au_2S domains remain intact under high pressure, nonhydrostatic stress at a range of 5.2−7.3 GPa (the pressure range of the CdS phase transition) can induce the breaking of Au−S covalent epitaxial bonds and chemically detach the small Au satellites from the HNC surfaces.[5] Further increasing the pressure would result in migration and coalescence of Au satellites due to the anisotropic deviatoric stress (Figure 4a−d).[5] Finally, this pressure-processing results in single-crystalline Au islands at the surfaces of CdS−Au_2S HNCs (Figure S9). Moreover, we did not observe the formation of 1D heterorods as we reported previously for the study of a quantum dot−Au (QD−Au) HNC system under pressure.[5] We attribute this difference to the different superstructural stabilities of the fcc HNC-SLs under pressure. While the fcc SLs can be held up to 8.5 GPa in the case of QD−Au host-satellite HNCs as reported previously,[5] the same fcc structure collapsed at a much lower pressure of ∼1.8 GPa in the case of CdS−Au_2S−Au Janus-satellite HNCs shown here (Figure 3a). This superstructural instability explains the absence of heterorod formation, which requires the preservation of fcc HNC-SLs during the Au-satellite detachment and migration processes under uniaxial compression (pressure range of ∼5−8 GPa).[5]

In conclusion, we demonstrated a unique fabrication of heterotrimer NCs through pressure processing where CdS−Au_2S−Au Janus-satellite HNCs went through interfacial Au−S bond breaking, followed by an intraparticle migration and coalescence of Au satellites under high pressure. Importantly, our study shows that pressure-driven synthesis can be generally applied to produce highly complex multicomponent HNCs beyond single and binary systems, bypassing conventional synthetic chemistry. The as-synthesized three-component HNCs are suitable for a range of applications including heterogeneous photocatalysis and multifunctional theranostics. This study not only provides a fundamental understanding of pressure-induced HNC transformations at atomic and meso scales but also paves the way for future pressure processing and fabrication of heterostructural nanomaterials with novel and unexplored architectures driven by the desired applications.

■ ASSOCIATED CONTENT

Supporting Information

The Supporting Information is available free of charge on the ACS Publications website at DOI: 10.1021/acsanm.9b01860.

Synthetic procedure, details of in situ SAXS/WAXS measurements, additional TEM characterization of HNCs before and after pressure, and detailed fitting results of SAXS/WAXS (PDF)

■ AUTHOR INFORMATION

Corresponding Author

*E-mail: ouchen@brown.edu.

ORCID

Hua Zhu: 0000-0003-2733-7837
Yucheng Yuan: 0000-0003-3935-0967
Xudong Wang: 0000-0002-1189-8181
Jing Zhao: 0000-0002-6882-2196
Ou Chen: 0000-0003-0551-090X

Author Contributions

The manuscript was written through contributions of all authors. All authors have given approval to the final version of the manuscript.

Notes

The authors declare no competing financial interest.

■ ACKNOWLEDGMENTS

O.C. acknowledges support from the Brown University startup fund. O.C. also is thankful for support from the National Science Foundation under Award CBET-1936223. J.Z. acknowledges partial financial support from the National Science Foundation (Grant CHE-1554800). This research used the CMS and FIS beamlines of the National Synchrotron Light Source II, a U.S. Department of Energy (DOE), Office of Science User Facility, operated for the DOE, Office of Science, by Brookhaven National Laboratory under Contract DE-SC0012704. Beamline 22-IR-1 is supported by COMPRES, the Consortium for Materials Properties Research in Earth Sciences under NSF Cooperative Agreement EAR 1606856 and the DOE/NNSA (DE-NA-0003858, CDAC). The STEM studies were performed using the facilities in the UConn/Thermo Fisher Scientific Center for Advanced Microscopy and Materials Analysis.

DOI: 10.1021/acsanm.9b01860
ACS Appl. Nano Mater. 2019, 2, 6804−6808

REFERENCES

(1) Cozzoli, P. D.; Pellegrino, T.; Manna, L. Synthesis, Properties and Perspectives of Hybrid Nanocrystal Structures. *Chem. Soc. Rev.* **2006**, *35* (11), 1195−1208.

(2) Habas, S. E.; Lee, H.; Radmilovic, V.; Somorjai, G. A.; Yang, P. Shaping Binary Metal Nanocrystals through Epitaxial Seeded Growth. *Nat. Mater.* **2007**, *6* (9), 692−697.

(3) Shi, W.; Zeng, H.; Sahoo, Y.; Ohulchanskyy, T. Y.; Ding, Y.; Wang, Z. L.; Swihart, M.; Prasad, P. N. A General Approach to Binary and Ternary Hybrid Nanocrystals. *Nano Lett.* **2006**, *6* (4), 875−881.

(4) Sun, Y. G. Interfaced Heterogeneous Nanodimers. *Natl. Sci. Rev.* **2015**, *2* (3), 329−348.

(5) Zhu, H.; Nagaoka, Y.; Hills-Kimball, K.; Tan, R.; Yu, L.; Fang, Y.; Wang, K.; Li, R.; Wang, Z.; Chen, O. Pressure-Enabled Synthesis of Hetero-Dimers and Hetero-Rods through Intraparticle Coalescence and Interparticle Fusion of Quantum-Dot-Au Satellite Nanocrystals. *J. Am. Chem. Soc.* **2017**, *139* (25), 8408−8411.

(6) Kim, D.; Shin, K.; Kwon, S. G.; Hyeon, T. Synthesis and Biomedical Applications of Multifunctional Nanoparticles. *Adv. Mater.* **2018**, *30* (49), 1802309.

(7) Kamat, P. V. Manipulation of Charge Transfer across Semiconductor Interface. A Criterion That Cannot Be Ignored in Photocatalyst Design. *J. Phys. Chem. Lett.* **2012**, *3* (5), 663−672.

(8) Jiang, R.; Li, B.; Fang, C.; Wang, J. Metal/Semiconductor Hybrid Nanostructures for Plasmon-Enhanced Applications. *Adv. Mater.* **2014**, *26* (31), 5274−5309.

(9) Waiskopf, N.; Ben-Shahar, Y.; Banin, U. Photocatalytic Hybrid Semiconductor-Metal Nanoparticles; from Synergistic Properties to Emerging Applications. *Adv. Mater.* **2018**, *30* (41), 1706697.

(10) Zhu, H.; Fan, Z.; Yuan, Y.; Wilson, M. A.; Hills-Kimball, K.; Wei, Z.; He, J.; Li, R.; Grunwald, M.; Chen, O. Self-Assembly of Quantum Dot-Gold Heterodimer Nanocrystals with Orientational Order. *Nano Lett.* **2018**, *18* (8), 5049−5056.

(11) Zhu, H.; Fan, Z.; Yu, L.; Wilson, M. A.; Nagaoka, Y.; Eggert, D.; Cao, C.; Liu, Y.; Wei, Z.; Wang, X.; He, J.; Zhao, J.; Li, R.; Wang, Z.; Grunwald, M.; Chen, O. Controlling Nanoparticle Orientations in the Self-Assembly of Patchy Quantum Dot-Gold Heterostructural Nanocrystals. *J. Am. Chem. Soc.* **2019**, *141* (14), 6013−6021.

(12) Boles, M. A.; Engel, M.; Talapin, D. V. Self-Assembly of Colloidal Nanocrystals: From Intricate Structures to Functional Materials. *Chem. Rev.* **2016**, *116* (18), 11220−11289.

(13) Schick, I.; Lorenz, S.; Gehrig, D.; Schilmann, A. M.; Bauer, H.; Panthofer, M.; Fischer, K.; Strand, D.; Laquai, F.; Tremel, W. Multifunctional Two-Photon Active Silica-Coated Au@MnO Janus Particles for Selective Dual Functionalization and Imaging. *J. Am. Chem. Soc.* **2014**, *136* (6), 2473−2483.

(14) Bradley, M. J.; Read, C. G.; Schaak, R. E. Pt-Au Nanoparticle Heterodimers as Seeds for Pt-Au-Metal Sulfide Heterotrimers: Thermal Stability and Chemoselective Growth Characteristics. *J. Phys. Chem. C* **2015**, *119* (16), 8952−8959.

(15) Nagaoka, Y.; Hills-Kimball, K.; Tan, R.; Li, R. P.; Wang, Z. W.; Chen, O. Nanocube Superlattices of Cesium Lead Bromide Perovskites and Pressure-Induced Phase Transformations at Atomic and Mesoscale Levels. *Adv. Mater.* **2017**, *29* (18), 1606666.

(16) Wang, Z.; Chen, O.; Cao, C.; Finkelstein, K.; Smilgies, D. M.; Lu, X.; Bassett, W. A. Integrating in Situ High Pressure Small and Wide Angle Synchrotron X-Ray Scattering for Exploiting New Physics of Nanoparticle Supercrystals. *Rev. Sci. Instrum.* **2010**, *81*, 093902.

(17) Xiao, G.; Cao, Y.; Qi, G.; Wang, L.; Liu, C.; Ma, Z.; Yang, X.; Sui, Y.; Zheng, W.; Zou, B. Pressure Effects on Structure and Optical Properties in Cesium Lead Bromide Perovskite Nanocrystals. *J. Am. Chem. Soc.* **2017**, *139* (29), 10087−10094.

(18) Li, Q.; Wang, Y.; Pan, W.; Yang, W.; Zou, B.; Tang, J.; Quan, Z. High-Pressure Band-Gap Engineering in Lead-Free $Cs_2AgBiBr_6$ Double Perovskite. *Angew. Chem., Int. Ed.* **2017**, *56* (50), 15969−15973.

(19) Jaffe, A.; Lin, Y.; Mao, W.; Karunadasa, H. I. Pressure-Induced Metallization of the Halide Perovskite $(CH_3NH_3)PbI_3$. *J. Am. Chem. Soc.* **2017**, *139* (12), 4330−4333.

(20) Wang, T.; Li, R.; Quan, Z.; Loc, W. S.; Bassett, W. A.; Xu, H.; Cao, Y.; Fang, J.; Wang, Z. Pressure Processing of Nanocube Assemblies toward Harvesting of a Metastable Pbs Phase. *Adv. Mater.* **2015**, *27* (31), 4544−4549.

(21) Ji, M.; Wang, H.; Gong, Y.; Cheng, H.; Zheng, L.; Li, X.; Huang, L.; Liu, J.; Nie, Z.; Zeng, Q.; Xu, M.; Liu, J.; Wang, X.; Qian, P.; Zhu, C.; Wang, J.; Li, X.; Zhang, J. High Pressure Induced in Situ Solid-State Phase Transformation of Nonepitaxial Grown Metal@ Semiconductor Nanocrystals. *J. Phys. Chem. Lett.* **2018**, *9* (22), 6544−6549.

(22) Li, B.; Wen, X.; Li, R.; Wang, Z.; Clem, P. G.; Fan, H. Stress-Induced Phase Transformation and Optical Coupling of Silver Nanoparticle Superlattices into Mechanically Stable Nanowires. *Nat. Commun.* **2014**, *5* (1), 4179.

(23) Wang, Z.; Schliehe, C.; Wang, T.; Nagaoka, Y.; Cao, Y. C.; Bassett, W. A.; Wu, H.; Fan, H.; Weller, H. Deviatoric Stress Driven Formation of Large Single-Crystal Pbs Nanosheet from Nanoparticles and in Situ Monitoring of Oriented Attachment. *J. Am. Chem. Soc.* **2011**, *133* (37), 14484−14487.

(24) Ren, L.; Huang, X. L.; Zhang, B.; Sun, L. P.; Zhang, Q. Q.; Tan, M. C.; Chow, G. M. Cisplatin-Loaded Au-Au_2s Nanoparticles for Potential Cancer Therapy: Cytotoxicity, in Vitro Carcinogenicity, and Cellular Uptake. *J. Biomed. Mater. Res., Part A* **2008**, *85A* (3), 787−796.

(25) Fenton, J. L.; Steimle, B. C.; Schaak, R. E. Tunable Intraparticle Frameworks for Creating Complex Heterostructured Nanoparticle Libraries. *Science* **2018**, *360* (6388), 513−517.

(26) Sullivan, G. A. Diffusion and Solubility of Cu in Cds Single Crystals. *Phys. Rev.* **1969**, *184* (3), 796−805.

(27) Yuan, Y.; Zhu, H.; Wang, X.; Cui, D.; Gao, Z.; Su, D.; Zhao, J.; Chen, O. Cu-Catalyzed Synthesis of CdZnSe-CdZnS Alloy Quantum Dots with Highly Tunable Emission. *Chem. Mater.* **2019**, *31* (7), 2635−2643.

(28) Morris, T.; Copeland, H.; Szulczewski, G. Synthesis and Characterization of Gold Sulfide Nanoparticles. *Langmuir* **2002**, *18* (2), 535−539.

(29) Ishikawa, K.; Isonaga, T.; Wakita, S.; Suzuki, Y. Structure and Electrical-Properties of Au_2S. *Solid State Ionics* **1995**, *79*, 60−66.

(30) Murray, C. B.; Kagan, C. R.; Bawendi, M. G. Synthesis and Characterization of Monodisperse Nanocrystals and Close-Packed Nanocrystal Assemblies. *Annu. Rev. Mater. Sci.* **2000**, *30*, 545−610.

(31) Tolbert, S. H.; Alivisatos, A. P. Size Dependence of a First-Order Solid-Solid Phase-Transition - the Wurtzite to Rock-Salt Transformation in Cdse Nanocrystals. *Science* **1994**, *265* (5170), 373−376.

(32) Santamaria-Perez, D.; Daisenberger, D.; Ruiz-Fuertes, J.; Marqueno, T.; Chulia-Jordan, R.; Muehle, C.; Jansen, M.; Rodriguez-Hernandez, P.; Munoz, A.; Johnson, E. R.; Otero-de-la-Roza, A. Gold(I) Sulfide: Unusual Bonding and an Unexpected Computational Challenge in a Simple Solid. *Chem. Sci.* **2019**, *10* (26), 6467−6475.

DOI: 10.1021/acsanm.9b01860
ACS Appl. Nano Mater. 2019, 2, 6804−6808